Long-range isotropic and dipolar spin-spin interactions in the square planar rotator model

E. Rastelli, S. Regina, A. Tassi, and A. Carbognani
Dipartimento di Fisica dell' Università, Istituto MASPEC del Consiglio Nazionale delle Ricerche, and Istituto Nazionale per la Fisica della Materia, Parco Area delle Scienze 7/A, 43100 Parma, Italy
(Received 19 April 2001; revised manuscript received 22 June 2001; published 6 February 2002)

The simultaneous presence of a long-range isotropic antiferromagnetic interaction decaying as $1/r^3$ (where r is the spin-spin distance) and of a dipolar interaction in the square planar rotator model is studied. The pure isotropic antiferromagnetic interaction does not support long-range order, at variance with the pure dipole interaction. The model is investigated analytically at low temperature and by Monte Carlo (MC) simulations at higher temperature. The Luttinger-Tisza method provides a ground-state configuration affected by continuous degeneracy. Thermal fluctuations accounted for by the linear spin-wave approximation lift the degeneracy and lead to *order by thermal disorder*. Different kinds of order are found going from a pure antiferromagnetic to a pure dipole interaction. The mechanism that restores long-range order is understood by using the renormalized spin-wave theory. The accidental soft mode related to the continuous degeneracy of the ground state is replaced by a temperature-dependent gap. Temperature-driven first-order phase transitions between different ordered phases are investigated via a Landau functional. The phase diagram of the model is obtained by study of the order parameter, specific heat, and staggered magnetization evaluated by MC simulations.

DOI: 10.1103/PhysRevB.65.094412 PACS number(s): 75.10.Hk, 75.30.Ds, 75.40.Mg

I. INTRODUCTION

The planar rotator model is a very peculiar system. Indeed it has no quantum counterpart and the absence of a third spin component prevents any dynamical feature. However, this model plays an important role in statistical physics. Indeed many actual magnetic systems with strong planar anisotropy are expected to share thermodynamic properties with the planar rotator model. When the spin-spin interaction in the model is restricted to nearest neighbor (NN) long-range order (LRO) is absent at any nonzero temperature,[1] but the topological Kosterlitz-Thouless (KT) phase transition[2] from a low-temperature phase characterized by divergent susceptibility to the paramagnetic phase is believed to occur on the basis of high-temperature series expansion,[3] renormalization group (RG) analysis,[2] and Monte Carlo (MC) simulations.[4,5]

Different scenarios appear when long-range interactions are accounted for. The dipole interaction is a long-range interaction of particular interest because it is occurs in any magnetic system. When the exchange interaction is strong, as for transition-metal compounds, the dipole interaction is simulated by a single-ion effective anisotropy.[6] This cannot be done when exchange and dipole interactions are of the same order of magnitude as it is for the rare-earth metal compounds of the $R\mathrm{Ba_2Cu_3O_7}$ family[7] where R is a rare-earth metal ion. In this paper we study a square planar rotator model with both long range isotropic antiferromagnetic and dipole interactions. In particular, we assume an antiferromagnetic coupling decaying as $1/r^3$ where r is the spin-spin distance.

The Hamiltonian of the model is

$$\mathcal{H}=-\frac{1}{2}\left(J_0+\frac{\mu^2}{a^3}\right)\sum_{\substack{i,\vec{r}\\ \vec{r}\neq 0}}\sum_{\alpha\beta} f^{\alpha\beta}(\vec{r})S_i^{\alpha}S_{i+\vec{r}}^{\beta}, \qquad (1.1)$$

where

$$f^{\alpha\beta}(\vec{r})=\frac{a^3}{r^3}\left(3\eta\frac{r^{\alpha}r^{\beta}}{r^2}-\delta_{\alpha,\beta}\right). \qquad (1.2)$$

$J_0>0$ is the isotropic antiferromagnetic interaction strength, a is the lattice constant, μ is the magnetic moment, i labels the sites of a square lattice, $\vec{r}$ is a generic lattice vector, α,β label x,y components, $\vec{S}_i$ is a two-component classical vector localized on site i, and $\eta=(\mu^2/a^3)/(J_0+\mu^2/a^3)$. As one can see $\eta=0$ corresponds to a pure long-range isotropic antiferromagnetic interaction and $\eta=1$ corresponds to a pure dipole interaction.

Linear spin-wave[8] (LSW) and renormalized spin-wave[9] (RSW) approximations suggest that no LRO is expected when $\eta=0$, in agreement with MC simulation.[8] A spin-wave argument suggests the existence of a low-temperature phase where LRO is absent but the susceptibility is divergent. The scenario changes when the long-range isotropic interaction is ferromagnetic. For such a model renormalization group analysis[10] as well as MC simulations[8,9] proves that LRO is assured. A pure dipole interaction is believed to support LRO on the basis of spin-wave analysis[9] and MC simulations.[9,11]

The ground state of the model Hamiltonian (1.1) is obtained by the Luttinger-Tisza[12] (LT) method in Sec. II. The ground state is affected by a continuous degeneracy. Indeed it is an antiferromagnetic two-sublattice Néel configuration where the direction of the sublattice magnetization is arbitrary for $0<\eta<0.210$. At $\eta=0.210$ one finds a change of the ground state leading to the same configuration found in the model with pure dipole interaction.[9] Indeed for $0.210<\eta<1$ a four-sublattice configuration appears where the spins of an elementary square (plaquette) make angles θ, $-\theta$, $\pi+\theta$, $\pi-\theta$ with the x axis, θ being arbitrary. The columnar phase corresponds to $\theta=0,\pi/2$. The LSW approximation provides contrasting indications about the effects of thermal fluctuations. Indeed the presence of a soft mode in the LSW energy spectrum, related to the continuous degen-

eracy of the ground state, leads to a divergent number of spin deviations so that no LRO is found. On the other hand, the LSW spectrum is θ dependent so that the ''harmonic'' free energy is θ dependent as shown in Sec. III. Order by thermal disorder[13] is strongly suggested. The minimum of the free energy for $0<\eta<0.210$ is found at $\theta=0(\pi/2)$, which corresponds to the antiferromagnetic (AF) Néel configuration with magnetic moments pointing along the x (y) axis. The rotational invariance of the pure isotropic model is destroyed by any dipole interaction. The columnar (C) phase is selected for $0.210<\eta<0.464$ and for $0.7675<\eta<1$. For $0.464<\eta<0.7675$ a vortical (V) configuration characterized by $\theta=\pi/4$ is selected. The columnar configuration found in the model with a pure dipole interaction[14,15] is recovered.

For $\eta=0$ and $\eta=1$ the RSW approach confirms the absence of LRO in the former case and provides LRO in the latter.[9] The soft mode for $\eta=0$ is related to the invariance under rotation of the model so that it survives thermal fluctuations and leads to a divergent number of spin deviations. On the contrary the accidental soft mode present in the LSW spectrum for $\eta=1$ is replaced by a temperature-dependent gap in the RSW approximation. LRO is assured even though an interesting nonanalytic behavior is found for vanishing temperature. An analogous result for $0<\eta<0.464$ and for $0.7675<\eta<1$ is found in Sec. IV. We believe that the appearence of a temperature dependent gap occurs also for $0.464<\eta<0.7675$ although the RSW approximation is untractable for vortical configurations since in this case the ground-state configuration cannot be described by a simple helix.

In Sec. V a Landau functional to describe the temperature-driven first-order columnar-vortical and vortical-columnar phase transition is proposed. A very small specific heat jump is found crossing the columnar-vortical or vortical-columnar phase boundary.

In Sec. VI the phase diagram of the model in the (η,T) plane is given as obtained by MC simulations. The order parameter, specific heat, and staggered susceptibility are evaluated for selected values of η. Critical exponents of the order parameter and of the staggered susceptibility are obtained by size scaling analysis of the MC data. The phase diagram consists of four regions corresponding to Néel (AF), columnar (C), vortical (V), and columnar (C) ordered phases. The model with $\eta=0$ appears to be an ''isolated'' point of the phase diagram. Indeed for any $\eta\neq 0$ the dipole interaction supports long-range order and the order-disorder transition temperature is finite. Section VII contains a summary and conclusions.

II. GROUND STATE

We apply the Luttinger-Tisza method[12] to the planar rotator model in order to get the ground-state spin configuration. We consider a square of four spins as basic array, the vertices of which are labeled 1,2,3,4. If Γ is the group of translations $l_1 a\mathbf{u}_x+l_2 a\mathbf{u}_y$ of the lattice and Γ^2 the subgroup of translations $2l_1 a\mathbf{u}_x+2l_2 a\mathbf{u}_y$, we consider the spin configurations obtained by applying Γ^2 to our basic arrays of spins. The energy of a generic spin configuration can be written as

$$U=-\frac{N}{8}\left(J_0+\frac{\mu^2}{a^3}\right)\sum_{\alpha=x,y}(S_1^\alpha S_2^\alpha S_3^\alpha S_4^\alpha)\times\begin{pmatrix} W_{00}^{\alpha\alpha} & W_{10}^{\alpha\alpha} & W_{11}^{\alpha\alpha} & W_{01}^{\alpha\alpha}\\ W_{10}^{\alpha\alpha} & W_{00}^{\alpha\alpha} & W_{01}^{\alpha\alpha} & W_{11}^{\alpha\alpha}\\ W_{11}^{\alpha\alpha} & W_{01}^{\alpha\alpha} & W_{00}^{\alpha\alpha} & W_{10}^{\alpha\alpha}\\ W_{01}^{\alpha\alpha} & W_{11}^{\alpha\alpha} & W_{10}^{\alpha\alpha} & W_{00}^{\alpha\alpha}\end{pmatrix}\begin{pmatrix} S_1^\alpha\\ S_2^\alpha\\ S_3^\alpha\\ S_4^\alpha\end{pmatrix}, \quad (2.1)$$

where

$$W_{mn}^{xx}=\sum_{l_1,l_2}\frac{1}{[(m+2l_1)^2+(n+2l_2)^2]^{3/2}}\times\left[3\eta\frac{(m+2l_1)^2}{(m+2l_1)^2+(n+2l_2)^2}-1\right] \quad (2.2)$$

and

$$W_{mn}^{yy}=\sum_{l_1,l_2}\frac{1}{[(m+2l_1)^2+(n+2l_2)^2]^{3/2}}\times\left[3\eta\frac{(n+2l_2)^2}{(m+2l_1)^2+(n+2l_2)^2}-1\right]. \quad (2.3)$$

When $m=n=0$ the term in the sum with $l_1=l_2=0$ has to be excluded. Owing to the symmetry relationship $W_{mn}^{xx}=W_{nm}^{yy}$, the eigenvalues of the two matrices appearing in Eq. (2.1) are the same. The dipole interaction matrix can be easily diagonalized because it has the same eigenvectors as the group of permutations P_t $(t=1,2,3,4)$ for four elements: $P_1=I$ (identity), $P_2=(1,2)(3,4)$, $P_3=(1,4)(2,3)$, and $P_4=(1,3)(2,4)$. The unnormalized eigenvectors are

$$q(1)=\begin{pmatrix}1\\1\\1\\1\end{pmatrix},\quad q(2)=\begin{pmatrix}1\\-1\\1\\-1\end{pmatrix},$$

$$q(3)=\begin{pmatrix}1\\1\\-1\\-1\end{pmatrix},\quad q(4)=\begin{pmatrix}1\\-1\\-1\\1\end{pmatrix}, \quad (2.4)$$

and a generic spin configuration can be written

$$\begin{pmatrix} S_1^\alpha\\ S_2^\alpha\\ S_3^\alpha\\ S_4^\alpha\end{pmatrix}=a_\alpha q(1)+b_\alpha q(2)+c_\alpha q(3)+d_\alpha q(4), \quad (2.5)$$

with $\alpha=x,y$ under the ''weak'' condition on the spin magnitude:

$$\sum_{\alpha=x,y}(a_\alpha^2+b_\alpha^2+c_\alpha^2+d_\alpha^2)=S^2. \quad (2.6)$$

The ground-state energy is obtained in correspondence to the maximum eigenvalue of the dipole interaction matrix. Note that no demagnetization corrections are to be considered because in two-dimensional (2D) models such corrections are proportional to the inverse of the linear dimension of the macroscopic sample. The eigenvalues are

$$\lambda_1 = W_{00}^{xx} + W_{01}^{xx} + W_{11}^{xx} + W_{10}^{xx} = 13.545\,\eta - 9.030, \quad (2.7)$$

$$\lambda_2 = W_{00}^{xx} - W_{01}^{xx} + W_{11}^{xx} - W_{10}^{xx} = -3.969\,\eta + 2.646, \quad (2.8)$$

$$\lambda_3 = W_{00}^{xx} - W_{01}^{xx} - W_{11}^{xx} + W_{10}^{xx} = 4.163\,\eta + 0.935, \quad (2.9)$$

$$\lambda_4 = W_{00}^{xx} + W_{01}^{xx} - W_{11}^{xx} - W_{10}^{xx} = -6.970\,\eta + 0.935, \quad (2.10)$$

so that the ground-state energy E_0 is

$$E_0 = -\frac{NS^2}{2}\left(J_0 + \frac{\mu^2}{a^3}\right)\lambda_2 \quad (2.11)$$

for $0 < \eta < 0.210$ and

$$E_0 = -\frac{NS^2}{2}\left(J_0 + \frac{\mu^2}{a^3}\right)\lambda_3 \quad (2.12)$$

for $0.210 < \eta < 1$. For $\eta = 0.210$ one has $W_{11}^{xx} = W_{10}^{xx}$ so that $\lambda_2 = \lambda_3$. The spin configuration for $0 < \eta < 0.210$ is a Néel two-sublattice antiferromagnetic one:

$$\begin{pmatrix} \vec{S}_1 \\ \vec{S}_2 \\ \vec{S}_3 \\ \vec{S}_4 \end{pmatrix} = S\cos\theta \begin{pmatrix} 1 \\ -1 \\ 1 \\ -1 \end{pmatrix} \mathbf{u}_x + S\sin\theta \begin{pmatrix} 1 \\ -1 \\ 1 \\ -1 \end{pmatrix} \mathbf{u}_y . \quad (2.13)$$

For $0.210 < \eta < 1$ the spin configuration is a four-sublattice one where the spins make angles θ, $-\theta$, $\pi+\theta$, $\pi-\theta$, with the x axis

$$\begin{pmatrix} \vec{S}_1 \\ \vec{S}_2 \\ \vec{S}_3 \\ \vec{S}_4 \end{pmatrix} = S\cos\theta \begin{pmatrix} 1 \\ 1 \\ -1 \\ -1 \end{pmatrix} \mathbf{u}_x + S\sin\theta \begin{pmatrix} 1 \\ -1 \\ -1 \\ 1 \end{pmatrix} \mathbf{u}_y . \quad (2.14)$$

Note that the coefficients satisfy the ''strong'' condition on the spin magnitude. As one can see from Eqs. (2.13) and (2.14) the ground-state configuration is affected by continuous degeneracy because θ is arbitrary as happens for pure dipole interactions.[9,16]

III. SPIN-WAVE THEORY: ORDER BY THERMAL DISORDER

Following Ref. 14 the Hamiltonian (1.1) can be expanded in a series of spin deviations

$$\mathcal{H} = E_0 + \mathcal{H}_2 + \mathcal{H}_3 + \mathcal{H}_4 + \cdots, \quad (3.1)$$

where E_0 is given by Eq. (2.11) for $0 < \eta < 0.210$ and by Eq. (2.12) for $0.210 < \eta < 1$. The bilinear contribution reads

$$\mathcal{H}_2 = \frac{1}{2}\left(J_0 + \frac{\mu^2}{a^3}\right) S^2 \sum_{\vec{q}} \sum_{ss'} \psi_{-\vec{q}}^{(s)} A_{\vec{q}}^{ss'} \psi_{\vec{q}}^{(s')}, \quad (3.2)$$

where $\psi_{\vec{q}}^{(s)}$ is the spatial Fourier transform of the angular deviation of the spin on the sth sublattice. For $0 < \eta < 0.210$ (Néel phase) the elements of the symmetric matrix $\mathbf{A}_{\vec{q}}$ are

$$A_{\vec{q}}^{11} = A_{\vec{q}}^{22} = A_{\vec{q}}^{33} = A_{\vec{q}}^{44} = W_{00}^{xx}(0) - W_{10}^{xx}(0) - W_{01}^{xx}(0) + W_{11}^{xx}(0) - W_{00}^{yy}(\vec{q})\cos^2\theta - W_{00}^{xx}(\vec{q})\sin^2\theta + W_{00}^{xy}(\vec{q})\sin(2\theta), \quad (3.3a)$$

$$A_{\vec{q}}^{12} = A_{\vec{q}}^{34} = W_{10}^{xx}(\vec{q})\sin^2\theta + W_{10}^{yy}(\vec{q})\cos^2\theta - W_{10}^{xy}(\vec{q})\sin(2\theta), \quad (3.3b)$$

$$A_{\vec{q}}^{13} = A_{\vec{q}}^{24} = -W_{11}^{xx}(\vec{q})\sin^2\theta - W_{11}^{yy}(\vec{q})\cos^2\theta + W_{11}^{xy}(\vec{q})\sin(2\theta), \quad (3.3c)$$

$$A_{\vec{q}}^{14} = A_{\vec{q}}^{23} = W_{01}^{xx}(\vec{q})\sin^2\theta + W_{01}^{yy}(\vec{q})\cos^2\theta - W_{01}^{xy}(\vec{q})\sin(2\theta). \quad (3.3d)$$

For $0.210 < \eta < 1$ (columnar phase) the elements of the symmetric matrix $\mathbf{A}_{\vec{q}}$ are

$$A_{\vec{q}}^{11} = A_{\vec{q}}^{33} = W_{00}^{xx}(0) + W_{10}^{xx}(0) - W_{01}^{xx}(0) - W_{11}^{xx}(0) - W_{00}^{yy}(\vec{q})\cos^2\theta - W_{00}^{xx}(\vec{q})\sin^2\theta + W_{00}^{xy}(\vec{q})\sin(2\theta), \quad (3.4a)$$

$$A_{\vec{q}}^{12} = A_{\vec{q}}^{34} = W_{10}^{xx}(\vec{q})\sin^2\theta - W_{10}^{yy}(\vec{q})\cos^2\theta, \quad (3.4b)$$

$$A_{\vec{q}}^{13} = W_{11}^{xx}(\vec{q})\sin^2\theta + W_{11}^{yy}(\vec{q})\cos^2\theta - W_{11}^{xy}(\vec{q})\sin(2\theta), \quad (3.4c)$$

$$A_{\vec{q}}^{14} = A_{\vec{q}}^{23} = -W_{01}^{xx}(\vec{q})\sin^2\theta + W_{01}^{yy}(\vec{q})\cos^2\theta. \quad (3.4d)$$

The matrix elements $A_{\vec{q}}^{22} = A_{\vec{q}}^{44}$ are obtained from $A_{\vec{q}}^{11}$ changing the sign of the last term on the right side. Analogously $A_{\vec{q}}^{24}$ is obtained from $A_{\vec{q}}^{13}$ changing the sign of the last term. The coefficients $W_{mn}^{\alpha\beta}(\vec{q})$ are defined as follows:

$$W_{mn}^{xx}(\vec{q}) = \sum_{l_1,l_2} \frac{\cos[(m+2l_1)aq_x]\cos[(n+2l_2)aq_y]}{[(m+2l_1)^2 + (n+2l_2)^2]^{3/2}} \times \left[3\eta \frac{(m+2l_1)^2}{(m+2l_1)^2 + (n+2l_2)^2} - 1\right], \quad (3.5)$$

$$W_{mn}^{yy}(\vec{q}) = \sum_{l_1,l_2} \frac{\cos[(m+2l_1)aq_x]\cos[(n+2l_2)aq_y]}{[(m+2l_1)^2 + (n+2l_2)^2]^{3/2}} \times \left[3\eta \frac{(n+2l_2)^2}{(m+2l_1)^2 + (n+2l_2)^2} - 1\right], \quad (3.6)$$

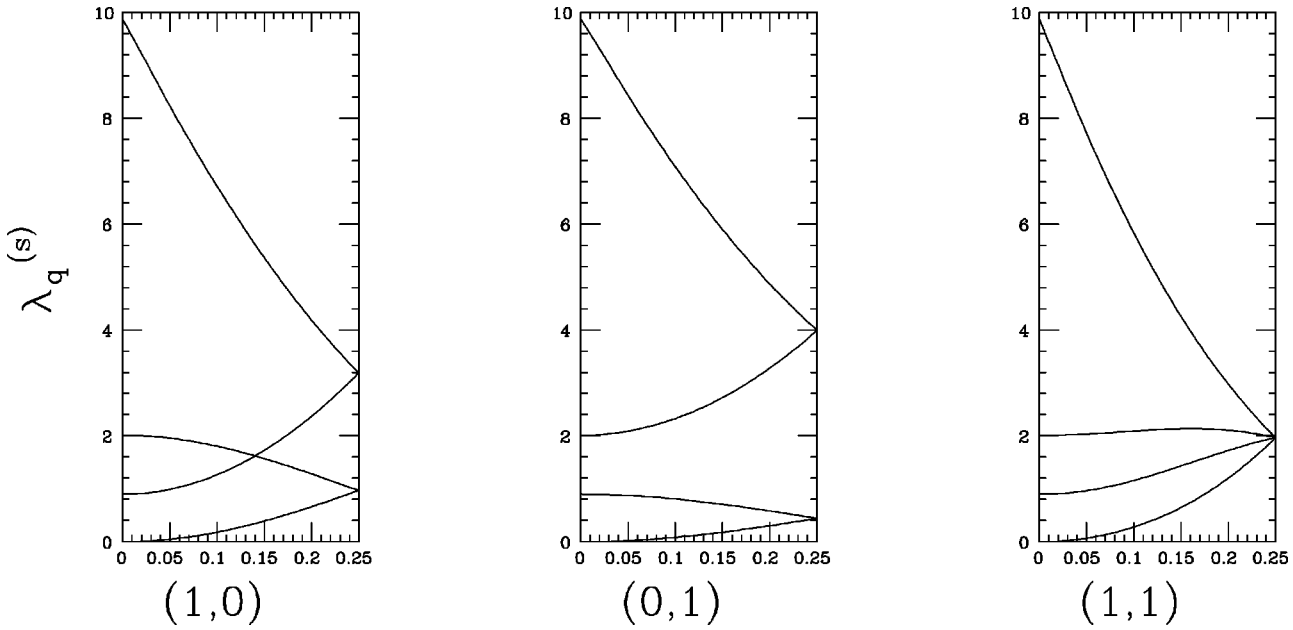

FIG. 1. Eigenvalues $\lambda_{\vec{q}}^{(s)}$ given by Eqs. (3.9) and (3.10) vs wave vector measured in reciprocal lattice units along the (1,0), (0,1), and (1,1) directions for $\eta=0.1$ and $\theta=0$. The spins are arranged in the antiferromagnetic (AF) Néel configuration.

$$W_{mn}^{xy}(\vec{q})=-\sum_{l_1,l_2}\frac{\sin[(m+2l_1)aq_x]\sin[(n+2l_2)aq_y]}{[(m+2l_1)^2+(n+2l_2)^2]^{3/2}}\times 3\eta\frac{(m+2l_1)(n+2l_2)}{(m+2l_1)^2+(n+2l_2)^2}. \tag{3.7}$$

When $m=n=0$ the term in the sum with $l_1=l_2=0$ has to be excluded. The eigenvalues $\lambda_{\vec{q}}^{(s)}$ of the matrix $\mathbf{A}_{\vec{q}}$ provide the LSW energy spectrum $\hbar\omega_{\vec{q}}^{(s)}$ for q_x,q_y ranging from $-\pi/2a$ to $\pi/2a$:

$$\hbar\omega_{\vec{q}}^{(s)}=\frac{1}{2}\left(J_0+\frac{\mu^2}{a^3}\right)S^2\lambda_{\vec{q}}^{(s)} \quad (s=1,2,3,4). \tag{3.8}$$

For $0<\eta<0.210$ the four eigenvalues $\lambda_{\vec{q}}^{(s)}$ are given by

$$\begin{aligned}\lambda_{\vec{q}}^{(1,2)}=&W_{00}^{xx}(0)-W_{10}^{xx}(0)-W_{01}^{xx}(0)+W_{11}^{xx}(0)\\&-[W_{00}^{yy}(\vec{q})+W_{11}^{yy}(\vec{q})]\cos^2\theta\\&-[W_{00}^{xx}(\vec{q})+W_{11}^{xx}(\vec{q})]\sin^2\theta\\&+[W_{00}^{xy}(\vec{q})+W_{11}^{xy}(\vec{q})]\sin(2\theta)\\&\mp\{[W_{10}^{xx}(\vec{q})+W_{01}^{xx}(\vec{q})]\sin^2\theta\\&+[W_{10}^{yy}(\vec{q})+W_{01}^{yy}(\vec{q})]\cos^2\theta\\&-[W_{10}^{xy}(\vec{q})+W_{01}^{xy}(\vec{q})]\sin(2\theta)\},\end{aligned} \tag{3.9}$$

$$\begin{aligned}\lambda_{\vec{q}}^{(3,4)}=&W_{00}^{xx}(0)-W_{10}^{xx}(0)-W_{01}^{xx}(0)+W_{11}^{xx}(0)\\&-[W_{00}^{yy}(\vec{q})-W_{11}^{yy}(\vec{q})]\cos^2\theta\\&-[W_{00}^{xx}(\vec{q})-W_{11}^{xx}(\vec{q})]\sin^2\theta+[W_{00}^{xy}(\vec{q})-W_{11}^{xy}(\vec{q})]\\&\times\sin(2\theta)\mp\{[W_{10}^{xx}(\vec{q})-W_{01}^{xx}(\vec{q})]\sin^2\theta\\&+[W_{10}^{yy}(\vec{q})-W_{01}^{yy}(\vec{q})]\cos^2\theta\\&-[W_{10}^{xy}(\vec{q})-W_{01}^{xy}(\vec{q})]\sin(2\theta)\}.\end{aligned} \tag{3.10}$$

As one can see the eigenvalues (3.9) and (3.10) are functions of the wave vector $\vec{q}$ and depend on the angle θ that characterizes the continuous degeneracy of the ground state. Figure 1 shows the eigenvalues $\lambda_{\vec{q}}^{(s)}$ versus $\vec{q}$ along some directions of high symmetry for $\eta=0.1$ and $\theta=0$.

For $0.210<\eta<1$ the eigenvalues $\lambda_{\vec{q}}^{(s)}$ become

$$\begin{aligned}\lambda_{\vec{q}}^{(1,2)}=&W_{00}^{xx}(0)+W_{10}^{xx}(0)-W_{01}^{xx}(0)-W_{11}^{xx}(0)\\&-[W_{00}^{yy}(\vec{q})+W_{11}^{yy}(\vec{q})]\cos^2\theta-[W_{00}^{xx}(\vec{q})+W_{11}^{xx}(\vec{q})]\\&\times\sin^2\theta\mp\{[(W_{10}^{xx}(\vec{q})+W_{01}^{xx}(\vec{q}))\sin^2\theta\\&-(W_{10}^{yy}(\vec{q})+W_{01}^{yy}(\vec{q}))\cos^2\theta]^2\\&+[W_{00}^{xy}(\vec{q})+W_{11}^{xy}(\vec{q})]^2\sin^2(2\theta)\}^{1/2}\end{aligned} \tag{3.11}$$

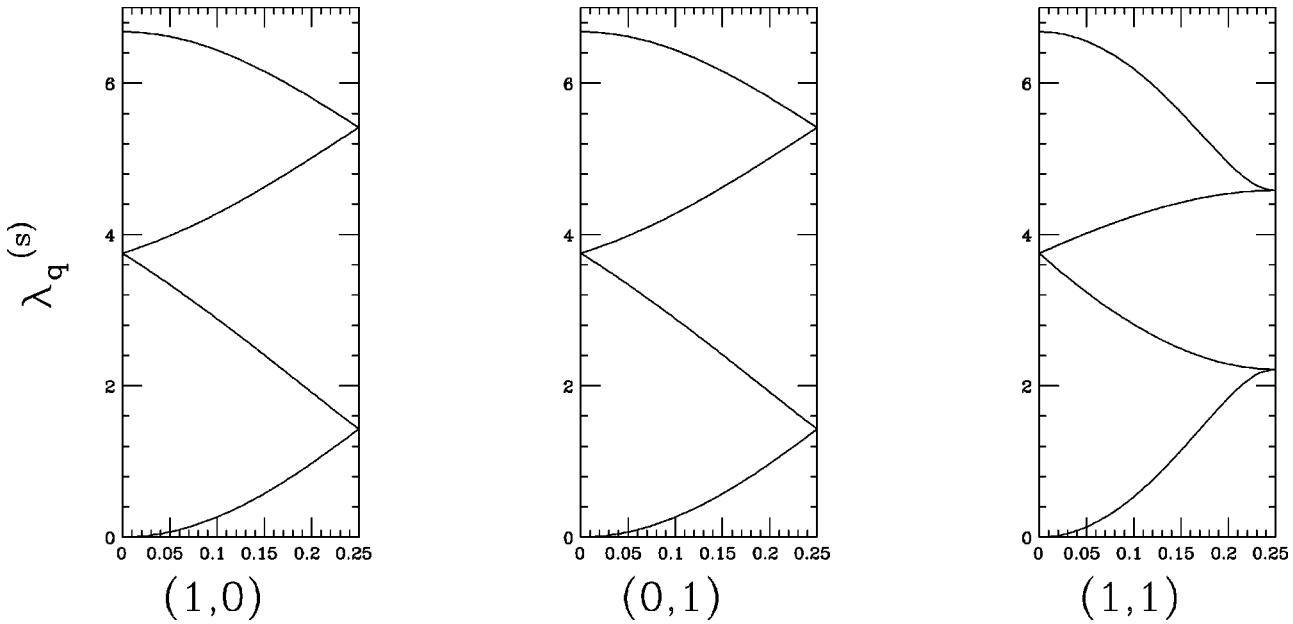

FIG. 2. Eigenvalues $\lambda_{\vec{q}}^{(s)}$ given by Eqs. (3.11) and (3.12) vs wave vector for $\eta=0.6$ and $\theta=\pi/4$. The spins are arranged in the vortical (V) phase.

$$\lambda_{\vec{q}}^{(3,4)} = W_{00}^{xx}(0) + W_{10}^{xx}(0) - W_{01}^{xx}(0) - W_{11}^{xx}(0) - [W_{00}^{yy}(\vec{q}) - W_{11}^{yy}(\vec{q})]\cos^2\theta - [W_{00}^{xx}(\vec{q}) - W_{11}^{xx}(\vec{q})]\sin^2\theta \mp \{[(W_{10}^{xx}(\vec{q}) - W_{01}^{xx}(\vec{q}))\sin^2\theta - (W_{10}^{yy}(\vec{q}) - W_{01}^{yy}(\vec{q}))\cos^2\theta]^2 + [W_{00}^{xy}(\vec{q}) - W_{11}^{xy}(\vec{q})]^2\sin^2(2\theta)\}^{1/2}. \quad (3.12)$$

Figure 2 shows the eigenvalues $\lambda_{\vec{q}}^{(s)}$ for $\eta=0.6$ and $\theta=\pi/4$.

Figure 3 shows the same quantities for $\eta=1$ and $\theta=0$. Note the existence of a soft mode for $\vec{q}\to 0$ in Figs. 1–3. One branch in each figure goes to zero quadratically in the long-wavelength limit. This peculiarity is true for any value of the angle θ.

In order to test the effect of thermal fluctuations on the spin configuration we evaluate the free energy in LSW approximation strictly following Ref. 14:

$$\mathcal{F} = -\frac{1}{2}\lambda - \frac{1}{2}T\ln\frac{T}{2\pi} + \frac{1}{2}Tf(\eta,\theta), \quad (3.13)$$

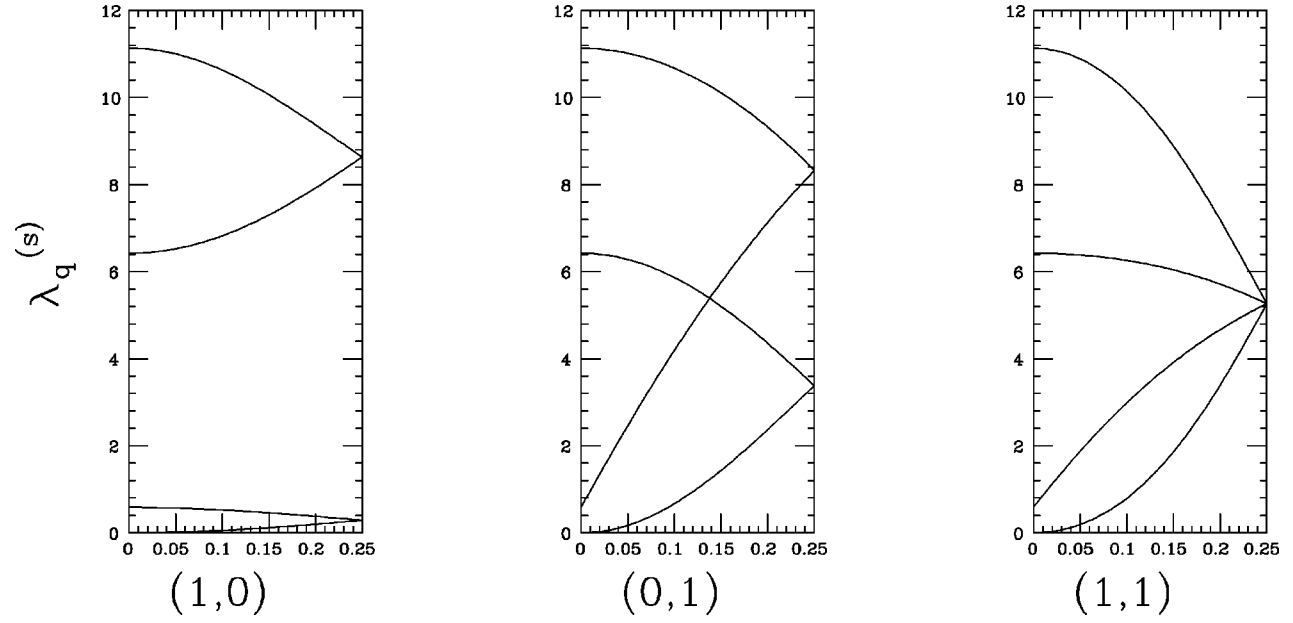

FIG. 3. Eigenvalues $\lambda_{\vec{q}}^{(s)}$ given by Eqs. (3.11) and (3.12) vs wave vector for $\eta=1$ and $\theta=0$. The spins are arranged in the columnar (C) phase.

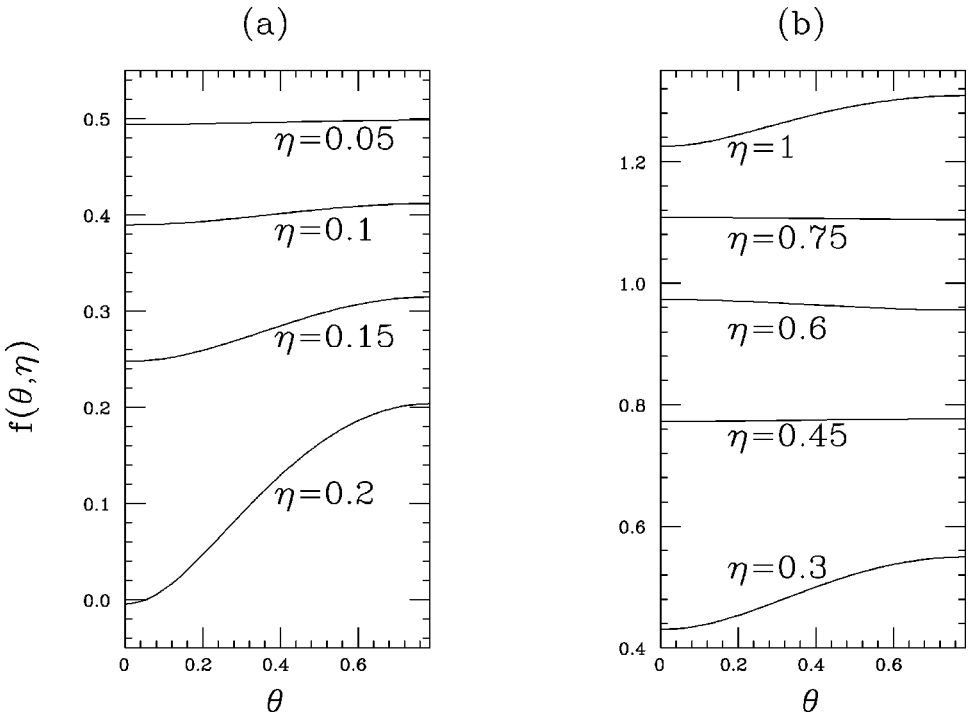

FIG. 4. The free energy θ-dependent term given by Eq. (3.14) vs θ for selected values of η (a) AF configuration and (b) columnar and vortical configuration.

where $\mathcal{F}$ is the reduced free energy per spin and T is reduced temperature in units $(J_0+\mu^2/a^3)S^2$, $\lambda=\lambda_2$ for $0<\eta<0.210$, $\lambda=\lambda_3$ for $0.210<\eta<1$, and

$$f(\eta,\theta)=\frac{a^2}{\pi^2}\int_0^{\pi/a}\int_0^{\pi/a}dq_x dq_y \ln(\det A_{\vec{q}}) = \frac{a^2}{\pi^2}\int_0^{\pi/a}\int_0^{\pi/a}dq_x dq_y \sum_{s=1}^{4}\ln\lambda_{\vec{q}}^{(s)}. \quad (3.14)$$

In Figs. 4 and 5, $f(\eta,\theta)$ is shown as a function of θ for different values of η. As one can see the minimum of the free energy occurs at $\theta=0$ for $0<\eta<0.464$ and $0.7675<\eta<1$, at $\theta=\pi/4$ for $0.464<\eta<0.7675$. The corresponding spin configurations are AF configuration [$\theta=0$ in Eq. (2.13)] for $0<\eta<0.210$, C configuration [$\theta=0$ in Eq. (2.14)] for $0.210<\eta<0.464$ and $0.7675<\eta<1$, V configuration [$\theta=\pi/4$ in (2.14)] for $0.464<\eta<0.7675$. This is a strong indication of *order by thermal disorder*.[13] Anyway the existence of one branch that vanishes quadratically as $\vec{q}$

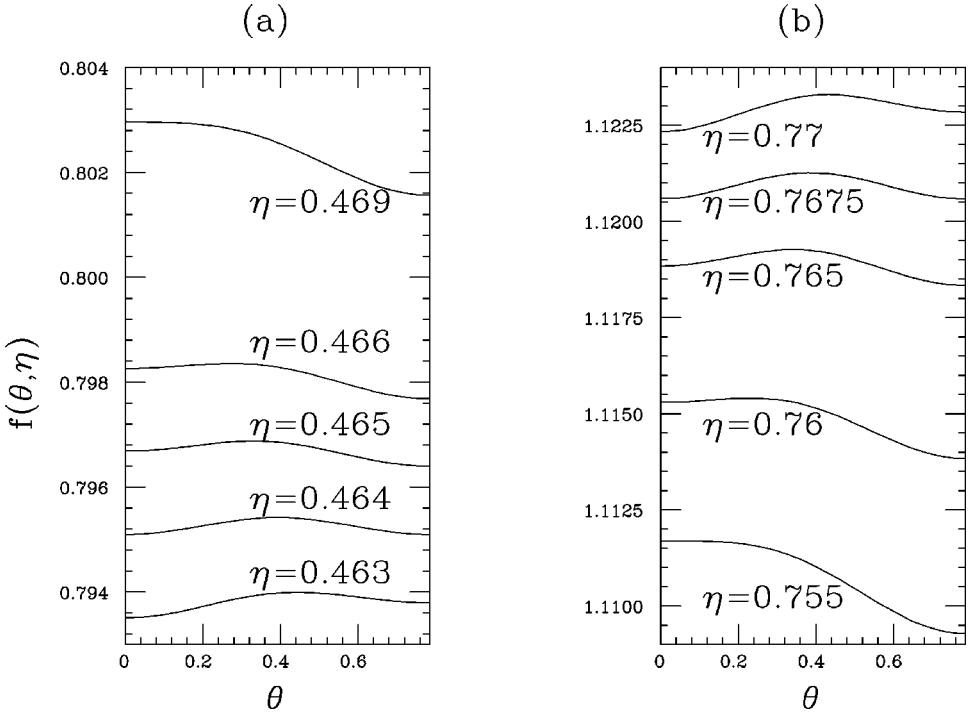

FIG. 5. The same as Fig. 4 for values of η (a) in the neighborhood of the first-order C-V phase transition occurring at $\eta=0.464$ (b) and in the neighborhood of the first-order V-C phase transition occurring at $\eta=0.7675$.

$\to 0$ for any η in the LSW spectrum leads to a divergent mean-square angular displacement as for the pure dipole interaction ($\eta=1$).[9] To understand the contrasting indications based on the free energy (3.13) and on the magnetization evaluated by the LSW approximation one has to go beyond the harmonic approximation.

For $\eta=0.210$ and $\theta=0$ (the angle selected by thermal fluctuations) the eigenvalues $\lambda_{\vec{q}}^{(s)}$ of the AF phase [Eqs. (3.9) and (3.10)] coincide with those of the columnar phase [Eqs. (3.11) and (3.12)]. Two very low quasidegenerate branches occur along the (0,1) direction. These two branches vanish quadratically for $\vec{q}\to 0$ and reach their maximum $\lambda_M=0.0161$ at the zone boundary $\vec{q}=(2\pi/a)(0,1/4)$. The existence of two soft modes for $\eta=0.210$ requires a self-consistent treatment of the anharmaonic contributions as shown in the next section.

IV. RENORMALIZED SPIN-WAVE THEORY

The LSW spectrum is $\hbar\omega_{\vec{q}}=\frac{1}{2}(J_0+\mu^2/a^3)S^2\epsilon_{\vec{q}}$ where

$$\epsilon_{\vec{q}}=D^{xx}(\vec{Q})-D^{yy}(\vec{Q}-\vec{q}) \tag{4.1}$$

for q_x, q_y ranging from $-\pi/a$ to π/a. Now the unit cell in the reciprocal lattice is the ''chemical'' cell which is 4 times larger than the ''magnetic'' cell. Of course $\epsilon_{\vec{q}}$ given by Eq. (4.1) reproduces the four branches given by Eqs. (3.9) and (3.10) for the AF phase and by Eqs. (3.11) and (3.12) for the C phase when the folding of the chemical cell is performed.

Note that the LSW spectrum vanishes at $\vec{q}=(0,0)$ in the AF phase where $\vec{Q}=(2\pi/a)(\frac{1}{2},\frac{1}{2})$ and at $\vec{q}_0=(2\pi/a)\times(\frac{1}{2},\frac{1}{2})$ in the C phase where $\vec{Q}=(2\pi/a)(0,\frac{1}{2})$. This fact implies the order parameter to be zero at any finite temperature. In analogy with the pure dipole case[17] we extend the RSW approximation to the case $\eta\neq 1$ in order to find a temperature-dependent gap that replaces the soft mode found in the LSW approximation.

The ground state of the AF phase for $0<\eta<0.210$ and of the C phase for $0.210<\eta<0.464$ and for $0.7675<\eta<1$ can be described by a regular helix of pitch $\vec{Q}=(2\pi/a)(\frac{1}{2},\frac{1}{2})$ and $\vec{Q}=(2\pi/a)(0,\frac{1}{2})$, respectively. This fact greatly simplifies the evaluation of the RSW spectrum. We apply the RSW approach to Hamiltonian (1.1) strictly following Ref. 17 where only the pure dipole interaction ($\eta=1$) was considered. Note that the cumulant expansion[17] selects the exact low-temperature leading contribution, so that the kind of LRO obtained by this approach is reliable. Equations (2.4)–(2.20) of Ref. 17 are directly extended to $\eta\neq 1$, replacing Hamiltonian (2.1) of Ref. 17 by Hamiltonian (1.1) of the present paper.

The so-obtained RSW spectrum is $\hbar\tilde{\omega}_{\vec{q}}=\frac{1}{2}(J_0+\mu^2/a^3)S^2\tilde{\epsilon}_{\vec{q}}$ where

$$\tilde{\epsilon}_{\vec{q}}=\epsilon_{\vec{q}}-T\Sigma(\vec{q}). \tag{4.2}$$

The renormalized gap in the AF phase [obtained for $\vec{q}=0$ and $\vec{Q}=(2\pi/a)(\frac{1}{2},\frac{1}{2})$] is

$$\Sigma_{AF}(0)=\frac{1}{N}\sum_{\vec{k}}\left[D^{xx}(\vec{Q}-\vec{k})-D^{yy}(\vec{Q}-\vec{k})\right]\frac{1}{\epsilon_{\vec{k}}}+\frac{2}{N}\sum_{\vec{k}}\left[\frac{D^{xy}(\vec{Q}-\vec{k})}{\epsilon_{\vec{k}}}\right]^2. \tag{4.3}$$

The renormalized gap in the C phase [obtained for $\vec{q}=\vec{q}_0$ and $\vec{Q}=(2\pi/a)(0,\frac{1}{2})$] is

$$\Sigma_C(\vec{q}_0)=\frac{1}{N}\sum_{\vec{k}}\left[D^{xx}(\vec{Q}+\vec{q}_0-\vec{k})-D^{yy}(\vec{Q}-\vec{k})\right]\frac{1}{\epsilon_{\vec{k}}}+\frac{1}{N}\sum_{\vec{k}}D^{xy}(\vec{Q}-\vec{k})\left[D^{xy}(\vec{Q}-\vec{k})+D^{xy}(\vec{Q}-\vec{k}+\vec{q}_0)\right]\frac{1}{\epsilon_{\vec{k}}}\frac{1}{\epsilon_{\vec{k}-\vec{q}_0}}. \tag{4.4}$$

Note that the soft modes in $\epsilon_{\vec{k}}$ at $\vec{k}=0$ in Eq. (4.3) and at $\vec{k}=\vec{q}_0$ in Eq. (4.4) do not make the sums divergent because of the simultaneous vanishing of the numerators. The self-energy (4.3) goes to zero as $\eta\to 0$ as expected because in the long-range isotropic antiferromagnetic system no gap exists owing to the presence of a genuine Goldstone mode related to the rotational invariance of the Hamiltonian. However, a temperature-dependent gap is expected for any $\eta\neq 0$ because of the symmetry breaking caused by the dipole interaction. For instance we obtain $\tilde{\epsilon}_0=0.102T$ at $\eta=0.1$. At $\eta=0.210$ one more soft mode appears at $\vec{q}=(2\pi/a)(0,1/2)$ in the AF phase and at $\vec{q}=(2\pi/a)(1/2,0)$ in the C phase. The two soft modes found at $\eta=0.210$ belong to the two soft branches discussed at the end of Sec. III. These two soft modes cause a divergence in the first sum of Eqs. (4.3) and (4.4), respectively. This is a signature of a nonanalytic behavior of the thermally renormalized gap as a function of temperature in the neighborhood of $\eta=0.210$. Perturbation theory fails and a self-consistent approach is required to solve the puzzle. The self-consistent renormalized gap for the AF phase is

$$\tilde{\epsilon}_0=-T\Sigma_{AF}(0,\tilde{\epsilon}_0), \tag{4.5}$$

where $\Sigma_{AF}(0,\tilde{\epsilon}_0)$ is obtained from Eq. (4.3) replacing $\epsilon_{\vec{k}}$ by $\epsilon_{\vec{k}}+\tilde{\epsilon}_0$. In the range $0<T<0.08$ the numerical solution of Eq. (4.5) is well fitted by the interpolation formula

$$\tilde{\epsilon}_0=-0.356T-0.635T\ln T. \tag{4.6}$$

The self-consistent renormalized gap for the columnar phase at $\eta=0.21$ is

$$\tilde{\epsilon}_{\vec{q}_0}=-T\Sigma_C(\vec{q}_0,\tilde{\epsilon}_{\vec{q}_0}), \tag{4.7}$$

where $\Sigma_C(\vec{q}_0,\tilde{\epsilon}_{\vec{q}_0})$ is given by Eq. (4.4) replacing $\epsilon_{\vec{k}}$ by $\epsilon_{\vec{k}}+\tilde{\epsilon}_{\vec{q}_0}$. In the range $0<T<0.03$ the interpolation formula is

$$\tilde{\epsilon}_{\vec{q}_0}=-2.879T-1.793T\ln T. \tag{4.8}$$

Away from $\eta=0.210$ the values of the renormalized gap obtained by the self-consistent or the perturbation approach are the same. For $\eta=0.3$ the perturbation theory provides $\tilde{\epsilon}_{\vec{q}_0}=0.652T$. At the C-V transition ($\eta=0.464$) the temperature-dependent gap becomes very small, $\tilde{\epsilon}_{\vec{q}_0}=0.0053T$. An analogous softening occurs at the V-C transition ($\eta=0.7675$) with $\tilde{\epsilon}_{\vec{q}_0}=0.0114T$. For $\eta=0.9$ we have $\tilde{\epsilon}_{\vec{q}_0}=0.210T$. Finally, for $\eta=1$ (pure dipole interaction) we recover the result of Ref. 17, namely, $\tilde{\epsilon}_{\vec{q}_0}=0.575T$. A calculation of the renormalized spectrum in the neighborhood of the wave vector corresponding to the gap gives

$$\tilde{\epsilon}_{\vec{q}} \simeq \epsilon_{GAP}(\eta)+c_x(\eta)q_x^2+c_y(\eta)q_y^2, \tag{4.9}$$

where $\epsilon_{GAP}(\eta)$ is $\tilde{\epsilon}_0$ for the AF phase and $\tilde{\epsilon}_{\vec{q}_0}$ for the C phase; c_x, c_y are finite for any η and are temperature independent at low temperature. The mean-square angular displacement becomes

$$\langle \psi_i^2 \rangle = \frac{T}{N}\sum_{\vec{k}} \frac{1}{\tilde{\epsilon}_{\vec{k}}} \simeq -\frac{1}{2\pi}\frac{1}{\sqrt{c_x c_y}} T \ln[\epsilon_{GAP}(\eta)]+\cdots, \tag{4.10}$$

where the ellipsis means regular terms linear in temperature coming from the regular contribution to the sum. This nonanalytic behavior was found also for the pure dipole interaction.[17] The order parameter

$$\langle \cos\psi_i \rangle = \cos(\vec{Q}\cdot\vec{r}_i) e^{-\langle \psi_i^2 \rangle/2} \tag{4.11}$$

has an infinite slope as $T\to 0$. In this limit the energy cost to create a spin wave of the wave vector in the neighborhood of the gap wave vector is vanishing so that a large number of spin waves can be excited. However, the interaction between spin waves originates a gap in the spectrum that increases at increasing temperature and LRO is restored. An isolated point exists $\eta=0$ for which $\epsilon_{GAP}(0)=0$ where LRO is absent as expected on the basis of the LSW approximation.[8] The actual thermal decreasing of the order parameter is strongly related to the LSW dispersion curve through c_x and c_y as it appears in Eqs. (4.10) and (4.11). For $\eta\to 0.210$ where two branches become very soft, we expect a decreasing of the order-disorder transition temperature in spite of the fact that the renormalized gap increases as $-T\ln T$ instead of T.

V. TEMPERATURE-DRIVEN FIRST-ORDER PHASE TRANSITION

The temperature-driven first-order phase transition was investigated by a Landau functional in the frame of the q-state Potts model in two dimensions with $q=10$.[18] We adopt an analogous approach to investigate the first-order columnar-vortical phase transition in the neighborhood of $\eta=0.464$ and $\eta=0.7675$ where the transition occurs at vanishing temperature. We are interested into the C-V phase boundary, in particular into the jump of the specific heat which could be peculiar since the C and V phases are supported by thermal fluctuations.

The free energy contribution for the Nèel, columnar, and vortical phases can be simulated by a Landau theory choosing a sixth-order functional

$$\mathcal{F}=\mathcal{F}_0+T\left(\frac{r}{2}\theta^2-\frac{u}{4}\theta^4+\frac{v}{6}\theta^6\right), \tag{5.1}$$

where

$$r=r_0+r_1T+r_2(\eta-\eta_0), \quad u,v>0. \tag{5.2}$$

and η_0 is the value at which a columnar-vortical (C-V) phase transition takes place in the low-temperature limit, r_1 is the coefficient of the anharmonic contribution to the free energy which is beyond the LSW approximation, and $\mathcal{F}_0$ is the free energy contribution independent of the angle θ characterizing the four-sublattice spin configuration. We have assumed the leading θ-dependent contribution to the free energy proportional to the temperature T in agreement with the result (3.13) obtained by LSW theory. Minimization of $\mathcal{F}$ with respect to θ provides the equilibrium spin configurations for the set of parameters r_0, r_1, r_2, u, v.

For $r<0$ the free energy (5.1) shows two minima at $\theta_0=\pm[(u+\sqrt{u^2-4vr})/2v]^{1/2}$ corresponding to a noncollinear phase we will identify with the vortical phase ($\theta_0=\pm\pi/4$) and a maximum at $\theta=0$ corresponding to the columnar phase.

For $0<r<u^2/4v$ the maximum at $\theta=0$ becomes a minimum so that the free energy exhibits three minima at $\theta=0$ (columnar phase) and $\theta_0=\pm[(u+\sqrt{u^2-4vr})/2v]^{1/2}$ (vortical phase) and two maxima at $\theta_M=\pm[(u-\sqrt{u^2-4vr})/2v]^{1/2}$. The simultaneous occurrence of minima at $\theta=0$ and $\theta=\theta_0$ is a minimal requirement to describe a first-order C-V phase transition which takes place when $\mathcal{F}(\theta=0)=\mathcal{F}(\theta=\theta_0)$, namely, for $r=3u^2/16v$. In the low-temperature limit and for η close to η_0 the above condition and Eq. (5.2) give

$$r_0=\frac{3u^2}{16v}, \quad T_c=-\frac{r_2}{r_1}(\eta_c-\eta_0). \tag{5.3}$$

For $r>u^2/4v$ the only minimum of Eq. (5.1) occurs at $\theta=0$ and corresponds to the columnar phase.

The C-V phase boundary $T_c=T_c(\eta_c)$ has a negative or positive slope depending on the sign of the ratio r_2/r_1 and whether η_c is greater or lesser than η_0.

The dimensionless specific heat $c=C/k_BL^2$ of the columnar and vortical phase is

$$c_I(\theta=0)=-T\frac{\partial^2\mathcal{F}_0}{\partial T^2} \tag{5.4}$$

and

$$c_{II}(\theta=\theta_0)=-T\frac{\partial^2\mathcal{F}_0}{\partial T^2}-r_1T\frac{u+\sqrt{u^2-4vr}}{2v}+\frac{r_1^2T^2}{2\sqrt{u^2-4vr}}, \tag{5.5}$$

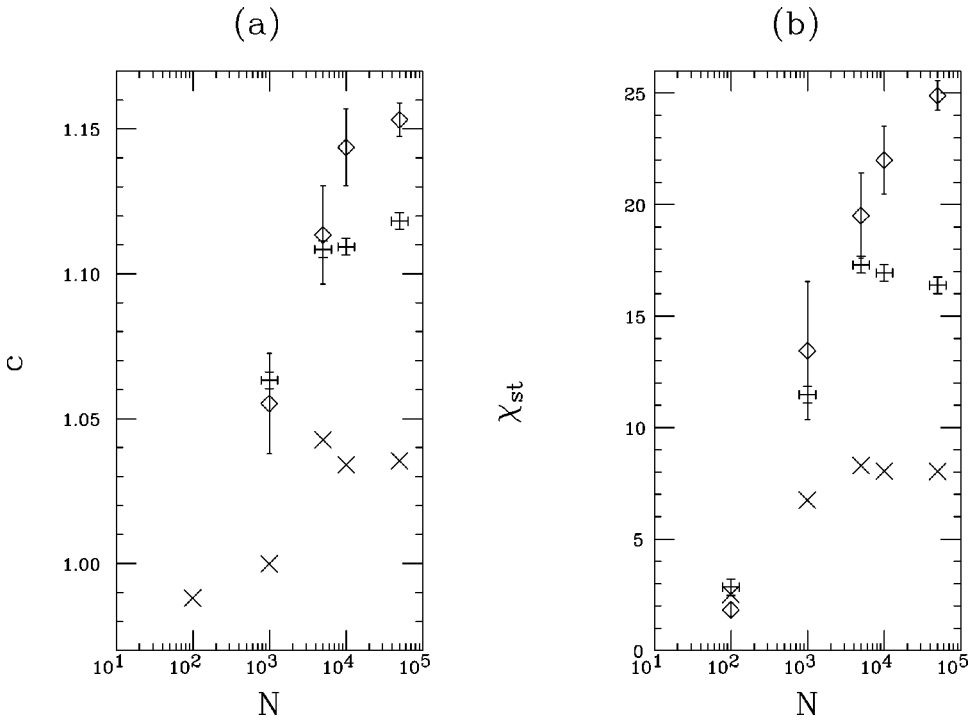

FIG. 6. (a) Specific heat at $\eta=1$ and $T=0.75$ for samples of size 16×16 (crosses), 24×24 (vertical crosses), and 32×32 (diamonds) as a function of N, where N is the number of configurations taken in the MC average. (b) The same for the staggered susceptibility. Error bars are shown only for the lattice of size 32×32.

respectively. At $T=T_c$, namely, for $r(T_c)=3u^2/16v$ and $\theta_0=\sqrt{3u/4v}$, the specific heat undergoes a jump discontinuity of magnitude

$$\Delta c = c_{II} - c_I \simeq r_2 \frac{3u}{4v}(\eta_c - \eta_0). \tag{5.6}$$

The set of parameters r_0, r_2, u, v are evaluated by fitting the sixth-order polynomial (5.1) with the free energy contribution (3.14) obtained by the LSW approximation and shown in Fig. 5. The first-order C-V phase transition takes place at $\eta_0=0.464$ for vanishing temperature with $r=r_0$ and $\theta=\theta_0$. In order to have $\theta_0=\pi/4$ one has to put $u/v=\pi^2/12$. The free energy barrier

$$[\mathcal{F}(\theta_M)-\mathcal{F}(\pi/4)]_{T=T_c}=[\mathcal{F}(\theta_M)-\mathcal{F}(0)]_{T=T_c}=T_c u\frac{\pi^4}{13824} \tag{5.7}$$

has to be compared with the LSW free energy (3.14) shown in Fig. 5 leading to $u=0.0227$. For η close to η_0 the free

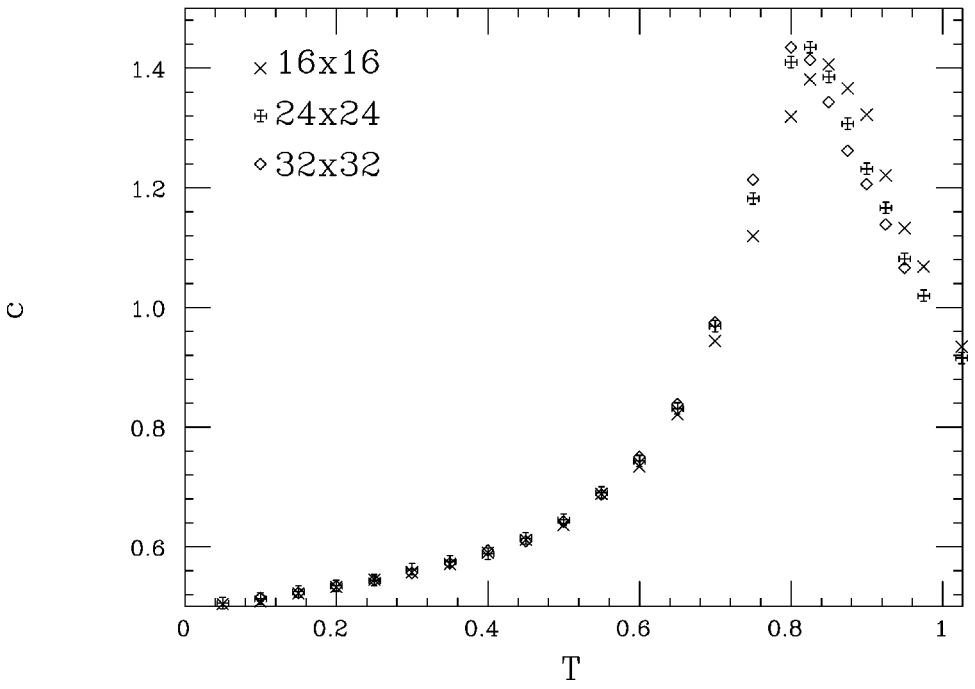

FIG. 7. Specific heat for $\eta=0.6$ as a function of temperature for lattice sizes of 16×16, 24×24, and 32×32 .

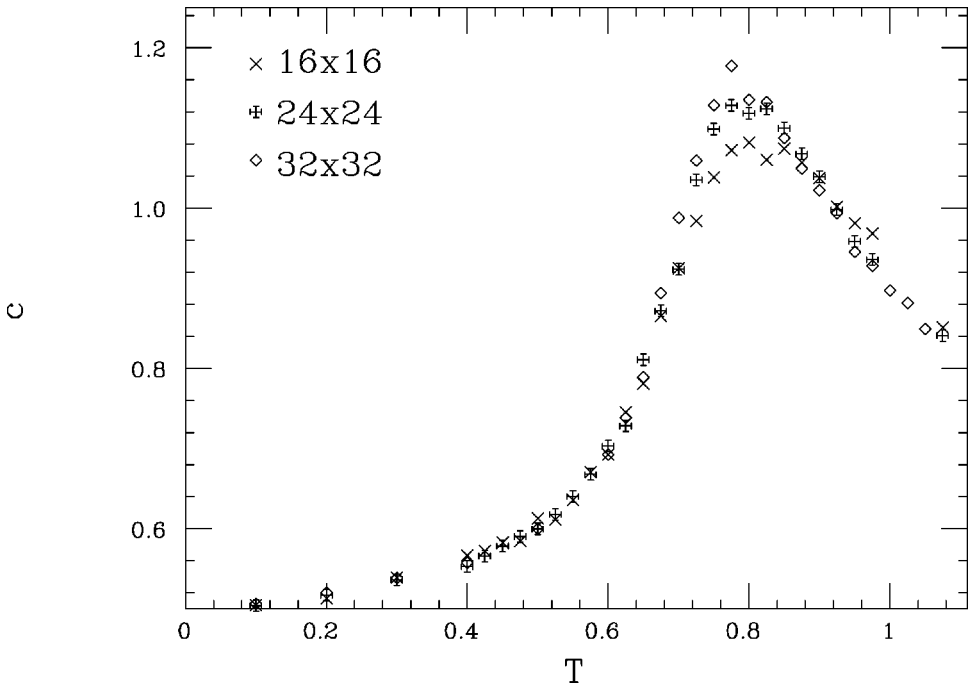

FIG. 8. The same as Fig. 7 for $\eta=1$.

energy difference between the vortical and columnar phase is

$$\mathcal{F}(\theta_0)-\mathcal{F}(0)=T\frac{\pi^2}{32}r_2(\eta-\eta_0). \tag{5.8}$$

A comparison with the LSW free energy difference $f(\eta,\pi/4)-f(\eta,0)$ shown in Fig. 5 gives $r_2\simeq-0.94$, $\Delta c \simeq 0.58(\eta_0-\eta_c)$, and $T_c=0.94/|r_1|(\eta_0-\eta_c)$. Note that the only unknown parameter is r_1 which is related to the anharmonic contribution to the free energy. Anyway r_1 must be negative in order to have a specific heat increasing with temperature in the low-temperature limit in agreement with the Monte Carlo simulation as we will see in the next section. The C-V phase boundary has a negative slope; namely, the C-V phase transition takes place for $\eta_c<\eta_0$ and specific heat shows a jump discontinuity at the transition.

Analogous fitting at $\eta_0=0.7675$ gives $u=0.047$ and $r_2 \simeq 0.65$ so that the jump discontinuity of the specific heat is $\Delta c\simeq 0.40(\eta_c-\eta_0)$ and the V-C phase boundary is $T_c=0.65/|r_1|(\eta_c-\eta_0)$. In this case the V-C phase boundary has a positive slope; namely, the phase transition takes place for $\eta_c>\eta_0$ and the specific heat shows a jump discontinuity at the transition.

VI. MONTE CARLO SIMULATION

We have performed MC simulations throughout the range $0\leqslant\eta\leqslant 1$ going from a pure isotropic antiferromagnetic long-range interaction to a pure dipole interaction. The approach of periodic ''images'' is adopted.[19] This approach, which is based on a periodic arrangement of MC cells, seems to be the most convenient to treat systems with long range interactions. The limiting cases $\eta=0$ and $\eta=1$ have been studied by MC simulations[17] and LRO was proved to exist in the former and prevented in the latter by performing a size scaling analysis of the mean-square angular displacement. In this section we evaluate the specific heat, order parameter, and staggered susceptibility for selected values of η in order to get the phase diagram of the model in the (η,T) plane.

We introduce a gauge tranformation[11] for the Néel phase,

$$\vec{M}=\sum_{l_1,l_2}(-1)^{l_1+l_2}[S_x(l_1,l_2)\mathbf{u}_x+S_y(l_1,l_2)\mathbf{u}_y], \tag{6.1}$$

and for the columnar and vortical phase,

$$\vec{M}=\sum_{l_1,l_2}[(-1)^{l_2}S_x(l_1,l_2)\mathbf{u}_x+(-1)^{l_1}S_y(l_1,l_2)\mathbf{u}_y]. \tag{6.2}$$

In order to suppress unphysical global rotation of the staggered magnetization due to the finite size of the sample we define the order parameter as

$$\psi=\langle|\vec{M}|\rangle/L^2, \tag{6.3}$$

where $L\times L$ is the number of lattice sites and $\langle\cdots\rangle$ means MC average. The order parameter (6.3) differs from that given in Ref. 17 where the average of the x component of the staggered magnetization was evaluated for $\eta=1$. We have tested the reliability of our MC data in the critical region evaluating the specific heat and staggered susceptibility at fixed temperature and different sample sizes as a function of the number of MC steps starting from the ground-state configuration as suggested by Ferrenberg *et al.*[20] In Figs. 6(a) and 6(b) the specific heat and staggered susceptibility evaluated for $\eta=1$, $T=0.75$, and different lattice sizes are shown as function of N, where N is the number of spin configurations used to evaluate the MC average. Each configuration is taken every ten MC steps. All data points in Figs. 6(a) and 6(b) are obtained by an average over ten independent MC

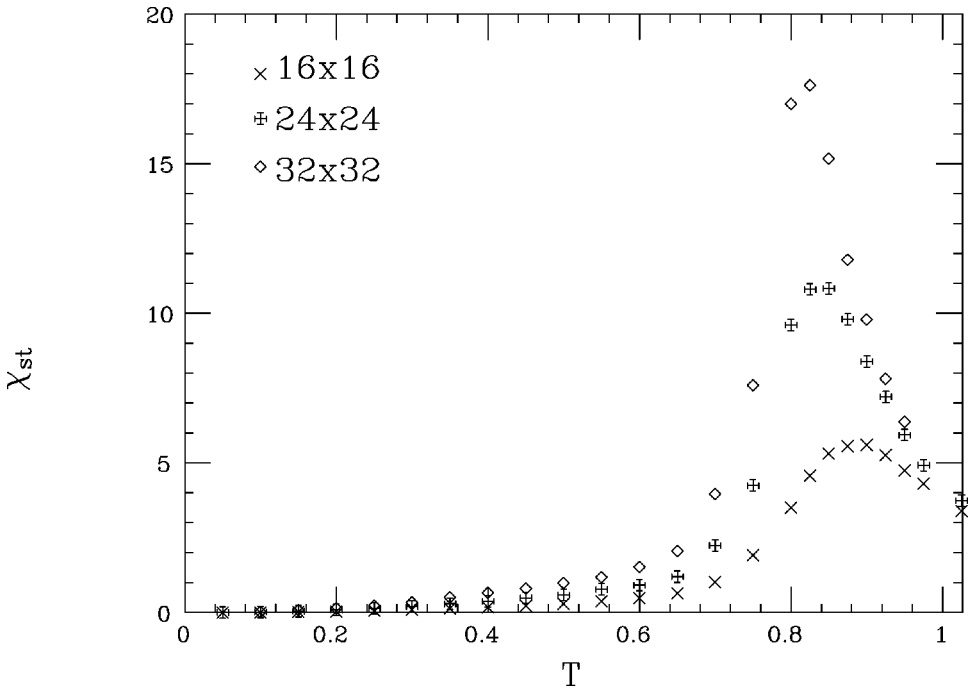

FIG. 9. Staggered susceptibility for $\eta=0.6$ as a function of temperature for lattice sizes of 16×16, 24×24, and 32×32.

runs. A plateau is obtained when N is sufficiently large for any lattice size. Larger N are required to reach saturation when the sample size increases. Asymptotic values of the specific heat and staggered susceptibility scale with the sample size as expected in the critical region of a continuous phase transition. A previous analysis is crucial in order to get information about the number of MC steps convenient to reach a good thermalization. In Figs. 7 and 8 we show the specific heat

$$c=\beta^2(\langle\mathcal{H}^2\rangle-\langle\mathcal{H}\rangle^2)/L^2 \tag{6.4}$$

versus temperature for $\eta=0.6$ and $\eta=1$ for different lattice sizes. All data points are an average over eight independent MC runs each of which consists of 10^4 MC configurations taken every ten MC steps. At each temperature 10^3 MC steps are discarded for thermalization assuming as starting configuration the final configuration of the previous temperature. This implies that a very long effective simulation is performed for temperatures belonging to the critical region. The pronounced peak of the specific heat shows a moderate scaling with the sample size whereas for temperatures far from the peak temperature MC data are size independent. In Figs. 9 and 10 the staggered susceptibility

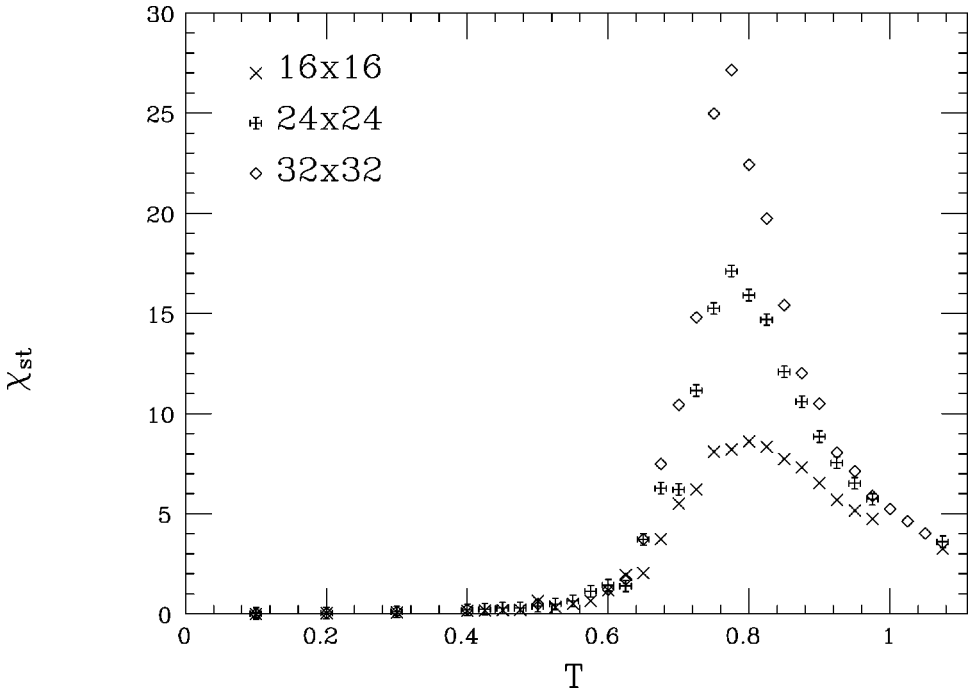

FIG. 10. The same as Fig. 9 for $\eta=1$.

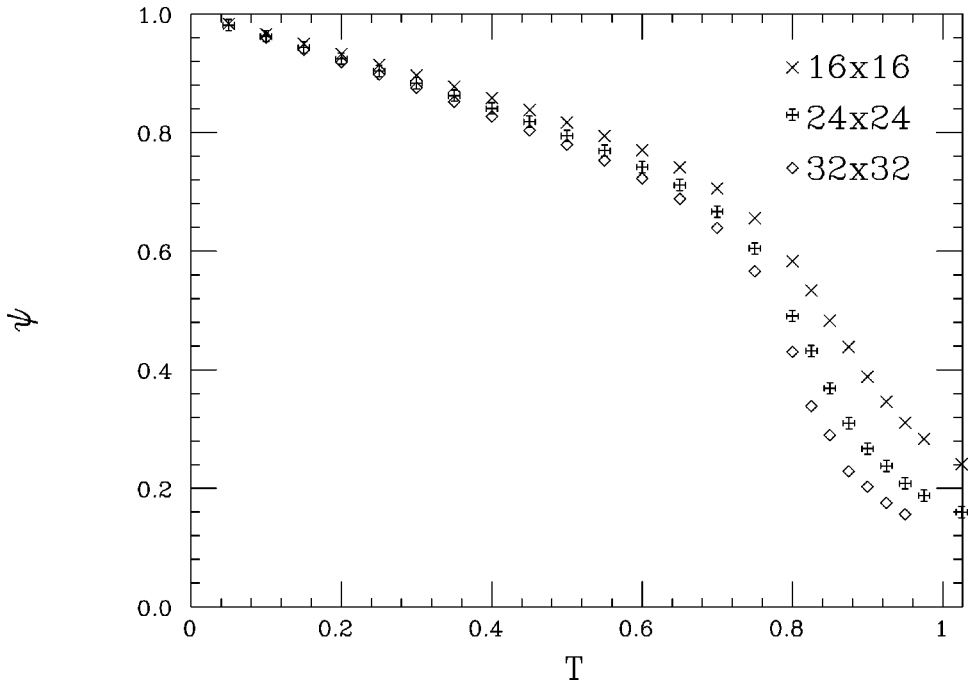

FIG. 11. Order parameter for $\eta=0.6$ as a function of temperature for lattice sizes of 16×16, 24×24, and 32×32.

$$\chi_{st}=(\langle|\vec{M}|^2\rangle-\langle|\vec{M}|\rangle^2)/L^2 \tag{6.5}$$

for the same values of η shows a sharp peak that scales with the sample size at the same temperature where the specific heat peak occurs. This is the signature of the occurrence of a continuous phase transition. The behavior of the order parameter (6.3) versus temperature shown in Figs. 11 and 12 supports the existence of this order-disorder transition. The location of the peaks of both specific heat and staggered susceptibility is slightly size dependent.

We have performed the size scaling analysis of the staggered susceptibility (6.5) and of the order parameter (6.3) for $\eta=1$, $\eta=0.6$, and $\eta=0.1$, corresponding to columnar, vortical, and Néel phases, in order to get critical exponents. We find that $\nu=1$ is consistent with the size scaling of the temperature at which the susceptibility reaches its maximum. The least-mean-squares method gives $\beta=0.26\pm0.03$ for all values of η and $\gamma=1.68\pm0.04$ for $\eta=1$ and $\eta=0.6$ while $\gamma=1.61\pm0.03$ for $\eta=0.1$. These values seem to be independent of the intensity of the isotropic exchange interaction. This is not surprising since the symmetry is the same for any $\eta\neq0$. Note that critical exponents for $\eta=1$ amend the results of Ref. 17 since in the present paper we have assumed a different order parameter to avoid the influence of unphysi-

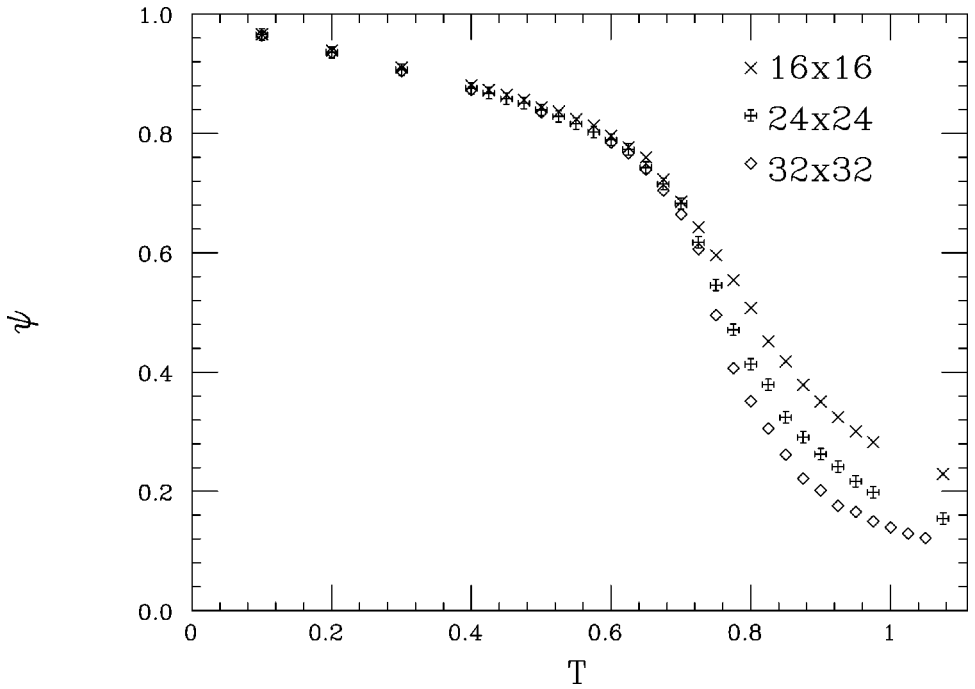

FIG. 12. The same as Fig. 11 for $\eta=1$.

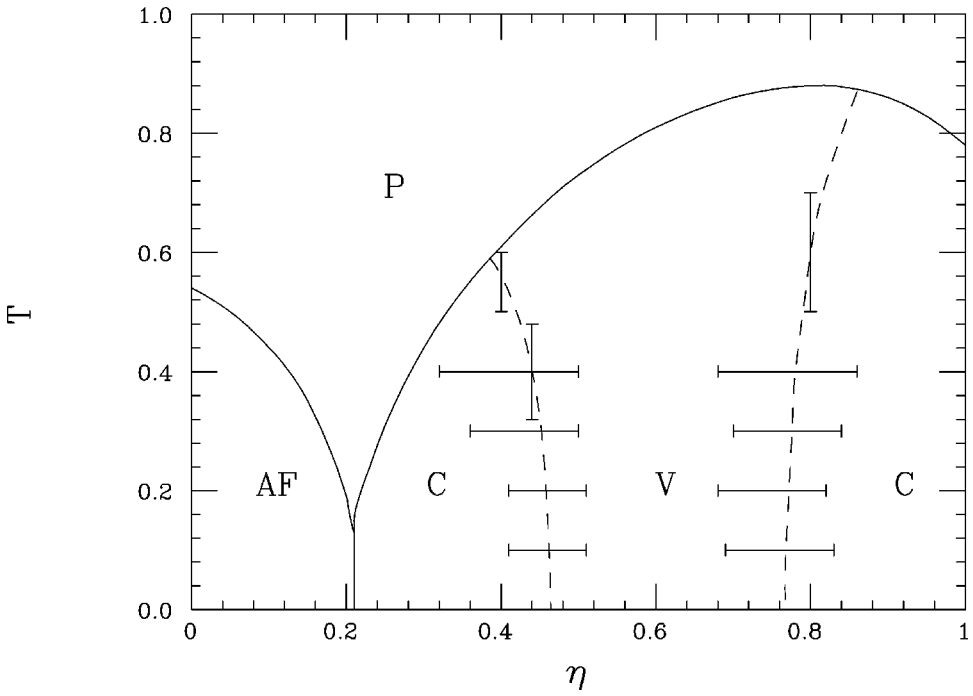

FIG. 13. Phase diagram in the (η,T) plane. AF, C, V, and P mean Néel antiferromagnetic, columnar, vortical, and paramagnetic configurations. Horizontal and vertical bars show the uncertainty of the C-V and V-C phase boundary locations.

cal global rotations. In any case we obtain critical exponents not falling in any known universality class. This fact is consistent with the conjectured correspondence[15] of the square planar model with a pure dipole interaction to the square planar model with nearest-neighbor interaction in presence of a fourfold-symmetry-breaking perturbation,[21] the critical exponents of which are believed to be dependent on the perturbation intensity.

In Fig. 13 the phase diagram of the model is shown in the (η,T) plane. The order-disorder phase boundary is drawn at the temperature $T_c(\eta)$ at which the specific heat and the susceptibility show their maximum. We have used a 24×24 sample averaging over $N=10^4$ of MC configurations as suggested by Fig. 6. The critical temperature undergoes a substantial decreasing in the neighborhood of $\eta=0.210$, as expected on the basis of the analytic result of Sec. IV. This is not the case of the C-V phase transition at $\eta=0.464$ and of the V-C phase transition at $\eta=0.7675$ where no soft branches in the energy spectrum are found.

The model with $\eta=0$ seems to be an isolated point. Indeed the critical temperature $T_c(\eta)$ of our finite sample with $L=24$ increases monotonically going from $\eta=0.210$ to $\eta=0$. On the other hand, our analytic calculation performed for $L\to\infty$ provides a logarithmic divergence of the mean-square angular displacement as given by Eq. (4.10). However, assuming a finite-size lattice the argument of the logarithm in Eq. (4.10) should be replaced by $\epsilon_{GAP}(\eta)+L^{-2}\simeq\eta T+L^{-2}$ so that values of η not lower than 10^{-2} have to be used to get reliable MC simulations.

The location of the two first-order phase boundaries between columnar and vortical phases is very difficult to determine. We have explored the regions around the C-V and V-C phase transitions for several temperatures evaluating $|\langle M_x\rangle|$ and $|\langle M_y\rangle|$ versus η using a 32×32 sample. Indeed one should have $|\langle M_x\rangle|\simeq1$ and $|\langle M_y\rangle|\simeq0$ in the columnar phase and $|\langle M_x\rangle|\simeq|\langle M_y\rangle|\simeq1/\sqrt{2}$ in the pure vortical phase for $T\to0$. In Figs. 14 and 15 we show $|\langle M_x\rangle|$ and $|\langle M_y\rangle|$ for $T=0.1$ around $\eta=0.46$ and $\eta=0.77$, respectively. The change of the spin configuration is clearly obtained but the location of the phase transition is affected by an error $\Delta\eta\simeq0.05$ around $\eta=0.46$ and $\Delta\eta\simeq0.08$ around $\eta=0.77$. Crosses and diamonds represent $|\langle M_x\rangle|$ and $|\langle M_y\rangle|$ for increasing η while squares and vertical crosses are the same for decreasing η. As one can see metastability effects are more pronounced around $\eta=0.77$. Analogous behavior was found for $T=0.2,0.3$, and 0.4. Horizontal bars in Fig. 13 show the uncertainty of the phase boundary location.

In Figs. 16 and 17 we show $|\langle M_x\rangle|$ and $|\langle M_y\rangle|$ versus temperature for $\eta=0.44$ and $\eta=0.8$, respectively. The C-V phase transition is obtained in both cases but it is not sharp and the uncertainty is shown by a vertical bar in Fig. 13. Similar behavior is found for $\eta=0.4$. On the contrary for $\eta=0.5,0.6,0.7,0.9$ no C-V phase transition occurs. These results allow us to draw the V-C phase boundaries (dashed lines) in Fig. 13. As one can see these phase boundaries are very steep. This implies a very small jump discontinuity of the specific heat across the phase boundaries on the basis of Eq. (5.6) so that it is not surprising that no evidence of a first-order phase transition is obtained from any MC simulation of the specific heat. On the basis of our analytical calculations proving the existence of ordered Néel, columnar, and vortical phases in the low-temperature limit and in agreement with MC simulation, we think that the phase diagram shown in Fig. 13 is reliable even though the order parameter data as a function of η shown in Figs. 14 and 15 do not undergo a steep increase prevented by the finite size of the sample.

VII. SUMMARY AND CONCLUSIONS

The square planar rotator model with a long-range isotropic interaction decaying as $1/r^3$ and dipole interaction is

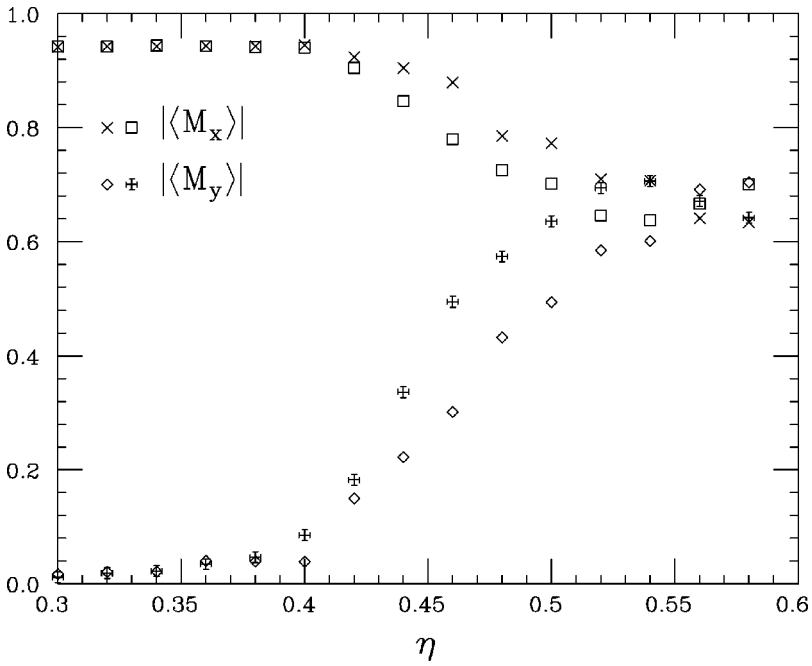

FIG. 14. $|\langle M_x\rangle|$ (crosses and squares) and $|\langle M_y\rangle|$ (diamonds and vertical crosses) vs η at $T=0.1$ around the C-V phase boundary. Crosses and diamonds correspond to the scan obtained by increasing η. Squares and vertical crosses correspond to the scan with decreasing η.

studied in the range $0<\eta<1$ where η measures the relative strength of the antiferromagnetic and dipole interaction. The Luttinger-Tisza method provides the ground-state configuration which is Néel, columnar, vortical, and columnar-like sweeping from $\eta=0$ to $\eta=1$. The ground state is affected by a continuous degeneracy corresponding to a free rotation of the sublattice magnetization with respect to the lattice. The low-temperature region is studied by the linear and renormalized spin-wave approximation. The continuous degeneracy is lifted at any nonzero temperature for any η and long-range order is supported by thermal fluctuations except for $\eta=0$ where no long-range order is found in agreement with MC simulations and RG analysis.

We have investigated the discontinuous columnar-vortical phase transition by a Landau functional simulating the θ-dependent free energy obtained by the LSW approach by a sixth-order polynomial. We have obtained the specific heat jump Δc and the C-V phase boundary. Very small Δc is expected but the actual slope of the C-V phase boundary depends on anharmonic contribution, which is beyond our analytical calculation.

We have performed MC simulations for selected values of η and we have evaluated the specific heat, staggered susceptibility, and order parameter. Critical exponents not falling in any known universality class are found by size scaling analysis of the MC data. The phase diagram agrees with the or-

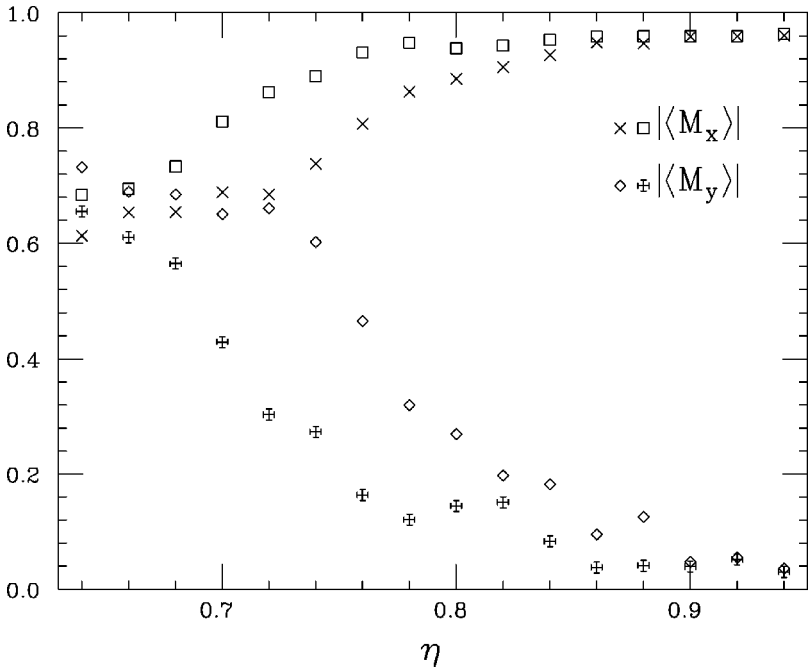

FIG. 15. The same as Fig. 14 around the V-C transition.

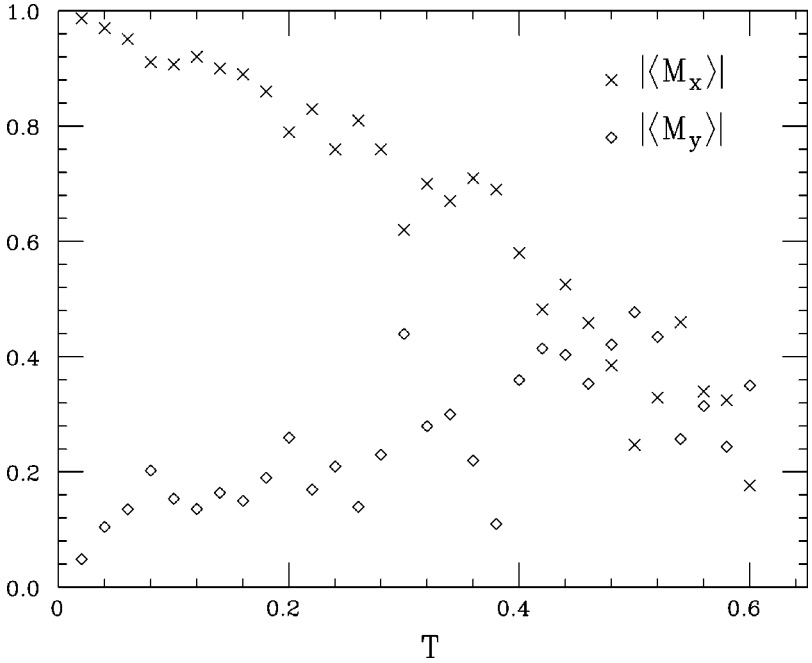

FIG. 16. $|\langle M_x \rangle|$ (crosses) and $|\langle M_y \rangle|$ (diamonds) vs T for $\eta = 0.44$.

dered phases found analytically in the low-temperature region. Size scaling of the specific heat and staggered susceptibility indicates that the order-disorder phase transition is continuous. The decreasing of the critical temperature around $\eta = 0.21$ where the Néel-columnar phase transition occurs is well understood in terms of the existence of two very low branches in the elementary excitation spectrum.

The columnar-vortical and vortical-columnar phase boundaries cannot be localized with the same precision as for the order-disorder phase boundary where a sharp peak in the specific heat and in the staggered suceptibility occurs. The columnar spin phase was observed in $ErBa_2Cu_3O_{6+x}$,[7] a compound where dipole forces play a crucial role owing to the weakness of the exchange interactions. Unfortunately the critical exponents were not measured so that we cannot test the values of β and γ we have obtained by size scaling analysis.

In summary a comprehensive study of the square planar model with long-range spin-spin interaction is presented. The long-range order is a consequence of thermal fluctuationsthat suppress unphysical Goldstone modes. MC simulations provide the phase diagram which agrees with the low-temperature analytic result.

ACKNOWLEDGMENT

The authors thank Professor David P. Landau for helpful discussions.

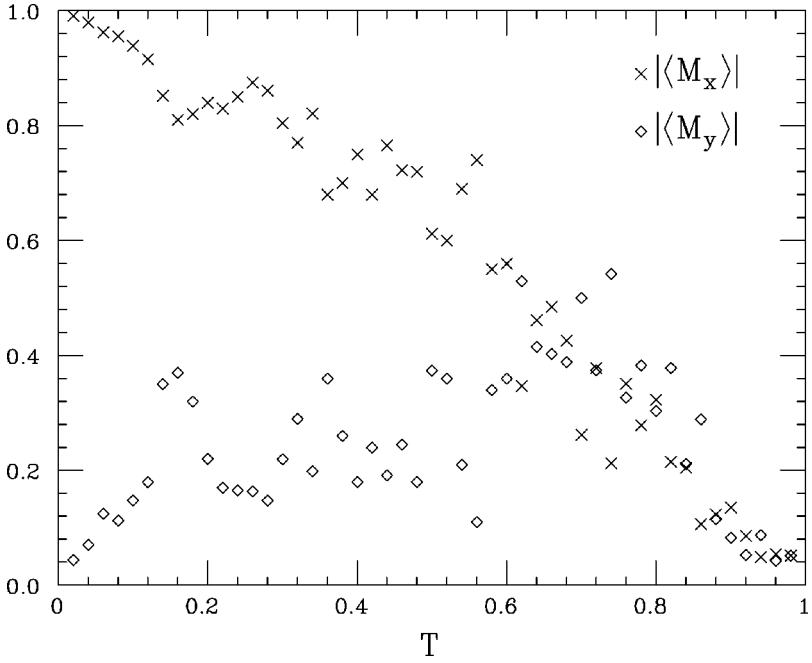

FIG. 17. The same as Fig. 16 for $\eta = 0.8$.

[1] N. D. Mermin and H. Wagner, Phys. Rev. Lett. **17**, 1133 (1966).
[2] J. M. Kosterlitz and D. J. Thouless, J. Phys. C **6**, 1181 (1973); J. M. Kosterlitz, *ibid.* **7**, 1046 (1974).
[3] P. Butera and M. Comi, Phys. Rev. B **47**, 11 969 (1993).
[4] J. F. Fernandez, M. F. Ferreira, and J. Stankiewicz, Phys. Rev. B **34**, 292 (1986).
[5] R. Gupta, J. DeLapp, G. G. Batrouni, G. C. Fox, C. F. Baillie, and J. Apostolakis, Phys. Rev. Lett. **61**, 1996 (1988).
[6] H. W. de Wijn, L. R. Walker, and R. E. Walstedt, Phys. Rev. B **8**, 285 (1973).
[7] S. Skanthakumar, J. W. Lynn, and F. Dogan, J. Appl. Phys. **81**, 4934 (1997); T. W. Clinton, J. W. Lynn, J. Z. Liu, Y. X. Jia, T. J. Goodwin, R. N. Shelton, B. W. Lee, M. Buchgeister, M. B. Maple, and J. L. Peng, Phys. Rev. B **51**, 15 429 (1995).
[8] S. Romano, Phys. Rev. B **44**, 7066 (1991).
[9] E. Rastelli, A. Carbognani, S. Regina, and A. Tassi, J. Appl. Phys. **85**, 6082 (1999).
[10] M. E. Fisher, S. Ma, and B. G. Nickel, Phys. Rev. Lett. **29**, 917 (1972).
[11] K. De'Bell, A. B. MacIsaac, I. N. Booth, and J. P. Whitehead, Phys. Rev. B **55**, 15 108 (1997).
[12] J. M. Luttinger and L. Tisza, Phys. Rev. **70**, 954 (1946).
[13] J. Villain, R. Bideaux, J. P. Carton, and R. Conte, J. Phys. (Paris) **41**, 1263 (1980); E. Rastelli, L. Reatto, and A. Tassi, J. Phys. C **16**, L331 (1983): C. L. Henley, Phys. Rev. Lett. **62**, 2056 (1989).
[14] E. Rastelli, A. Carbognani, S. Regina, and A. Tassi, Eur. Phys. J. B **9**, 641 (1999).
[15] S. Prakash and C. L. Henley, Phys. Rev. B **42**, 6574 (1990).
[16] P. I. Belobrov, R. S. Gekht, and V. A. Ignatchenko, Sov. Phys. JETP **57**, 636 (1983).
[17] A. Carbognani, E. Rastelli, S. Regina, and A. Tassi, Phys. Rev. B **62**, 1015 (2000).
[18] M. S. S. Challa, P. D. Landau, and K. Binder, Phys. Rev. B **34**, 1841 (1986).
[19] R. Kretschmer and K. Binder, Z. Phys. B **34**, 375 (1979).
[20] A. M. Ferrenberg, D.P. Landau, and K. Binder, J. Stat. Phys. **63**, 867 (1991).
[21] J. V. José, L. P. Kadanoff, S. Kirkpatrick, and D. R. Nelson, Phys. Rev. B **16**, 1217 (1977).